Open Archive TOULOUSE Archive Ouverte (OATAO)

OATAO is an open access repository that collects the work of Toulouse researchers and makes it freely available over the web where possible.

This is an author-deposited version published in : http://oatao.univ-toulouse.fr/
Eprints ID : 11114

Modelling epilithic biofilms combining hydrodynamics, invertebrate grazing and algal traits

MYRIAM GRABA*,†,‡, SABINE SAUVAGE*,†, NABIL MAJDI†,§, BENOÎT MIALET†,§,¶,
FRÉDÉRIC Y. MOULIN**,††, GEMMA URREA‡‡, EVELYNE BUFFAN-DUBAU†,§, MICHÈLE TACKX†,§,
SERGI SABATER‡‡,§§ AND JOSÉ-MIGUEL SANCHEZ-PÉREZ*,†

*Université de Toulouse, INP, UPS, EcoLab, Castanet Tolosan, France
†CNRS, EcoLab, Toulouse, France
‡Université Abderrahmane Mira, Bejaia, Algeria
§Université de Toulouse, INP, UPS, EcoLab, Toulouse, France
¶Littoral Environnement et Sociétés, UMR 7266 CNRS-Université de La Rochelle, La Rochelle, France
**Université de Toulouse, INP, ENSEEIHT, UPS, IMFT, Toulouse, France
††CNRS, IMFT, Toulouse, France
‡‡Faculty of Sciences, Institute of Aquatic Ecology, University of Girona, Girona, Spain
§§Catalan Institute for Water Research (ICRA), Girona, Spain

SUMMARY

1. This model of stream epilithic biofilm biomass dynamics is based on the system of equations from Uehlinger *et al.* (1996) and the term for autogenic detachment of biofilm from Boulêtreau *et al.* (2006). Its new features are (i) a mathematical term based on estimated feeding activity of biofilm-dwelling invertebrates, (ii) local hydrodynamics considered as the principal factor governing algal traits and biofilm structure and (iii) a variable degree of parameterisation that was adjusted to biofilm biomass conditions.

2. Biofilm biomass was monitored over a one-year period in the Garonne river in France (September 2008–2009). An allometric approach was used to estimate the feeding activity of biofilm-dwelling invertebrates based on their energetic requirements. Diatom functional diversity was also monitored to find how it varied with overall biofilm growth patterns. The one-year monitoring period was divided into six biofilm biomass cycles, with each cycle consisting of a phase of biofilm growth as the main process, followed by detachment.

3. This model reproduced the observed data as a complex of biofilm growth/detachment cycles using different sets of empirical parameters which allowed (i) the dominant processes involved in each biofilm cycle to be evaluated and (ii) the six cycles of biofilm growth/detachment to be reproduced. This accounted for the observed patterns more effectively than a parameterisation using a single set of empirical parameters.

4. High flow had a severe effect on biofilm dynamics through chronic and catastrophic detachment. Presumably as a result, assemblages of diatoms shifted towards species that were firmly attached and protected by mucilage.

5. During low flow (and when temperature was high), biofilm dynamics was mainly affected by autogenic detachment and grazer activity. The grazing pressure of the dominant biofilm-dwelling invertebrates (Nematoda and larvae of Chironomidae and Trichoptera) was fairly low (a maximum of 6% of biofilm biomass ingested daily); nevertheless, their presence in the biofilm seemed to favour biofilm autogenic detachment.

Keywords: diatoms, epilithic biofilm, grazing, local hydrodynamics, meiofauna

Correspondence: Myriam Graba and Sabine Sauvage, ENSAT/EcoLab, Avenue de l'Agrobiopôle, 31326 Castanet Tolosan, Toulouse, France.
E-mails: mgraba@yahoo.fr and sabine.sauvage@univ-tlse3.fr

Introduction

'Epilithic biofilms' are complex communities that grow on hard, submerged substrata and include algae, bacteria, fungi and microfauna embedded within a polymeric matrix (Lock *et al.*, 1984). Algae generally account for more than 30% of total biofilm biomass (Peterson, 1996) and can influence both the biomass (Sobczak, 1996) and diversity of bacteria (Jackson, Churchill & Roden, 2001) by providing nutrients and physical habitats. These biofilm communities have been studied widely because they play a major role in fluvial ecosystems by influencing primary production (Lock *et al.*, 1984), secondary production (Fuller, Roelofs & Frys, 1986; Winterbourn, 1990), decomposition (Ford & Lock, 1987) and nutrient retention (Mulholland *et al.*, 1991).

Environmental factors drive the structure and dynamics of stream biofilms. In particular, hydrodynamics heavily constrains epibenthic assemblages such as epilithic biofilms (Power & Stewart, 1987; Biggs, Nikora & Snelder, 2005). For instance, flow affects biofilm metabolic rate and the transfer of metabolites by limiting the thickness of the diffusive boundary layer of the mat (Riber & Wetzel, 1987; Costerton *et al.*, 1995; Chang *et al.*, 2003). Hydrology also affects the biofilm community structure by determining exchanges with the water column and ecological succession on substrata (Peterson & Stevenson, 1992; Tekwani *et al.*, 2013). In return, biofilm-dwelling organisms can affect the local architecture of the mat, resulting in reduced water velocity at the substratum–water interface, which reduces biofilm vulnerability to shear stress (Graba *et al.*, 2013). In other words, stream biofilm communities can be viewed as 'ecosystem engineers', modulating their microenvironment and reducing flow stress (Battin *et al.*, 2003; Besemer *et al.*, 2009). Mounting evidence also suggests that biofilms can buffer the effects of flow intermittency by sheltering aquatic communities from desiccation and spates (Costerton *et al.*, 1995; Peterson, 1996; Romani *et al.*, 2013; Timoner *et al.*, 2012). The frequency of hydrological extremes is expected to rise with climate change, exacerbated by flow abstraction (Lehner *et al.*, 2006), affecting ecosystem processes and community structure in the river. Thus, we need to understand biofilm dynamics more effectively, particularly with regard to their role in biogeochemical cycles and other 'ecosystem services'.

The biological assemblages composing epilithic biofilms, and the many environmental gradients and ecosystem processes within the mat, make this a very complex system. This complexity makes experimental explorations particularly challenging (Moulin *et al.*, 2008; Graba *et al.*,

2010, 2013). Mathematical models are therefore particularly useful tools for assessing our understanding quantitatively. In recent years, mathematical models have been developed to describe the dynamics of epilithic biofilm biomass, the earliest and simplest models related biofilm biomass to environmental variables, such as nutrient concentration, light intensity, temperature and hydrodynamics (*e.g.* McIntire, 1973, 1983; McIntire & Colby, 1978; Horner & Welch, 1981; Horner, Welch & Veenstra, 1983; Momo, 1995; McIntire *et al.*, 1996; Uehlinger, Buhrer & Reichert, 1996; Saravia, Momo & Boffi Lissin, 1998). The main processes involved in these models can be summarised by the equation: $dB/dt = C + G - D$, where B is the biomass, C a colonisation function, G is growth and D a detachment function [describing chronic, autogenic (self-generated) or catastrophic detachment, or a combination of these]. These models were developed either to explain processes observed in natural streams and rivers (Uehlinger *et al.*, 1996; Saravia *et al.*, 1998), or applied to artificial channels and laboratory streams (McIntire, 1973). In some cases, the processes of colonisation and growth were not modelled separately (Horner & Welch, 1981; Horner *et al.*, 1983; Uehlinger *et al.*, 1996), or the detachment process was ignored (Momo, 1995). The process of grazing by vertebrates and invertebrates has been modelled in hierarchical models proposed by McIntire & Colby (1978), McIntire (1983) and McIntire *et al.* (1996).

More recently, Asaeda & Hong Son (2000, 2001) presented a relatively complex biofilm model that incorporates layers of filamentous and non-filamentous species of algae with two different functions of growth and detachment for each functional type. Another complex model was that of Flipo *et al.* (2004), in which the growth of epilithic biomass was considered to be the same as for phytoplankton, but with two different equations for nitrifying and heterotrophic bacteria. Further models by Moulin *et al.* (2008) and Graba *et al.* (2010, 2012, 2013) have shown that, in experimental flumes, the resistance of biofilm to detachment is a function of local hydrodynamics in the boundary layer in which the biofilm grows. However, with the exception of models by McIntire & Colby (1978), McIntire (1983) and McIntire *et al.* (1996), these models consider neither grazing by biofilm-dwelling invertebrates, which can greatly alter biofilm growth (Hillebrand, 2009), nor ecological succession and competition among algal species and between algae and bacteria, which can modify the cohesion of the epilithic matrix facing flow stress (*e.g.* Stevenson, 1983; Jackson *et al.*, 2001).

In this context, an 'updated' biofilm dynamics model is proposed here, with components that can be

parameterised describing (i) local hydrodynamic constraints, (ii) feeding of biofilm-dwelling invertebrates and (ii) the taxonomic and functional composition of a dominant algal group (here, diatoms) to fill gaps in previous models and to evaluate the dominant processes involved in biofilm biomass dynamics.

Methods

Study site

The Garonne River (south-west France) is relatively large (eighth order, 647 km long) and has cobble bars covered with biofilm even in reaches up to the seventh order. The epilithic biofilm was sampled at a cobble bar 36 km upstream of the city of Toulouse where the Garonne is sixth order (latitude 01°17′53″E; longitude 43°23′45″N; altitude 175 m asl). The mean daily discharge in the Garonne fluctuates widely at Toulouse, ranging between 30 and 3500 m^3 s^{-1} (2001–2009). During the low water period (July–October), mean discharge is 50 m^3 s^{-1} and the river is shallow (<1.5 m) and wide (c. 100 m) with a mean current velocity around 0.5 m s^{-1} (Boulêtreau et al., 2006).

Epilithic biofilm biomass

Sampling ($n = 39$ sampling occasions) was undertaken approximately every 7–10 days from September 2008 to September 2009. On each occasion, four randomly selected cobbles were collected by hand and slid into plastic bags underwater to prevent any biofilm detachment during removal. Cobbles were collected at a depth between 30 and 50 cm, along a 50-m stretch of river (Améziane et al., 2002). The cobbles were transported to the laboratory within 2 h and with minimum disturbance, and the biofilm was then scraped from the upper surface of each using a scalpel and toothbrush. The scrapings were then suspended in 25 mL of ultrapure water (MilliQ filtration; Millipore, Billerica, MA, U.S.A.). Biofilm suspensions were dried (105 °C, 18 h), weighed and combusted (450 °C, 8 h) to assess the ash-free dry mass (AFDM) content. To express AFDM per unit area, scraped cobbles were photographed and the surface from which biofilm had been removed was measured (ImageJ software, version 1.38; Abramoff, Magelhaes & Ram, 2004).

Biofilm diatom community

Diatom species composition was determined from four cobbles collected at approximately monthly intervals (13

sampling occasions). Biofilm was scraped from the upper surface using a sterile toothbrush and suspended in 50 mL ultrapure water. The biofilm suspension was preserved with formaldehyde (4% final concentration). Only diatoms were considered and identified because of their dominance in the biofilm algal community at the study site (Leflaive et al., 2008; Majdi et al., 2011). Diatom cell contents were digested with HCl (37%) and subsequently heated at 100 °C for 2 h with H_2O_2. The heating step was repeated twice, and the cleaned frustules were rinsed on a 0.2-μm pore filter and finally suspended in 1–3 mL ultrapure water. A subsample of 200 μL was pipetted onto a coverslip and permanently preserved in Naphrax® mounting medium (Northern Biological Supplies, Ipswich, U.K.). For each sample, at least 400 diatoms were counted under a light microscope at 1000× magnification, identified to species and classified by functional diatom type (colonial, filamentous, fixed unicellular and free unicellular) based on Krammer & Lange–Bertalot (1991) and Leflaive et al. (2008). Data were expressed as the relative abundance of species (%). The proportion of live diatoms was assumed to be high because of the high chlorophyll a/phaeopigment ratio (averaging 36.5) observed during the study period (Majdi et al., 2012b).

Biofilm-dwelling invertebrates and estimation of their grazing pressure

On each sampling occasion, the biofilm organic fraction was extracted from four additional replicate cobbles using a modified gravity gradient centrifugation technique involving Ludox HS-40, after Pfannkuche & Thiel (1988), then poured through a 40-μm-mesh sieve. The biofilm-dwelling organisms retained on the sieve (comprising meio- and macroinvertebrates) were then preserved in formaldehyde (4% final concentration) and stained with 1% rose bengal. At least 200 organisms were counted per replicate subsample in a Dolfuss cell (Elvetec services, Clermont-Ferrand, France) under a stereomicroscope (9–90×) to determine their density. Nematodes (mostly Chromadorina spp.) and larvae of Chironomidae and Trichoptera (mostly Psychomyiidae) were the most significant groups in terms of biomass. Their individual biomass was measured in terms of dry mass content (DM) as follows: for each sample, at least 20 Chironomidae and 10 Trichoptera larvae were isolated in small aluminium cups and dried for 48 h at 50 °C to weigh their DM. The DM of at least 100 nematodes was assessed after biometric conversions of their body dimensions, assuming a specific gravity of 1.13

(Andrássy, 1956). Group biomass was calculated as the mean individual biomass multiplied by group density. Daily production P_d (mg DM m^{-2} day^{-1}) of nematodes, Chironomidae and Trichoptera larvae was calculated in accordance with Plante & Downing's (1989) regression. This method provides more reliable estimates of invertebrate production than other regressions available in the literature (Butkas, Vadeboncoeur & Vander Zanden, 2011). Total community daily production was calculated as the sum of the daily production of the various groups. The consumption of biofilm by each invertebrate group was calculated from their estimated nutritional needs (or total food needs TFN$_{Gr}$): TFN$_{Gr}$ = P_d/ (AE × NPE), where AE is the assimilation efficiency (assimilation/ingestion) and NPE is the net production efficiency (production/assimilation) of the invertebrates. AE = 0.3 and NPE = 0.4 after Benke & Wallace (1980) and Hall, Likens & Malcom (2001).

Environmental variables and hydrodynamic measurements

Mean daily discharge was supplied by a gauging station of the French water authorities (DIREN Midi-Pyrénées) located 10 km upstream of the study site. Global daily radiation was provided by a meteorological station 20 km NE of the study site. Daily radiation was first converted to daily integrated photosynthetically (400–700 nm) active radiation: PAR (J cm^{-2}) after Steemann-Nielsen (1975). In line with Uehlinger *et al.* (1996), PAR was then converted to photon flux density I (E m^{-2}). Mean daily temperature was calculated from hourly measurements using an automated probe (YSI 6000; Yellow Springs Instruments, Yellow Springs, OH, U.S.A.), placed 5 cm above the stream bed at the study site. Flow velocity and water depth were measured weekly at three points surrounding the area where the cobbles were sampled, using a flow metre (Flo-Mate 2000; Flow-Tronic, Welkenraedt, Belgium). The mean longitudinal velocity U_{moy} was estimated as an average value of the measured velocities 2.5 cm from the bottom and at 40 and 80% of the water column height with respective weight factors of 1, 2 and 1. Daily water depth values h (m) were interpolated or extrapolated from a logarithmic correlation between the weekly measured water depth and the corresponding mean daily discharge Q (m^3 s^{-1}): $h = 0.27 \ln(Q)^{-0.61}$ (R^2 = 0.71, n = 20 measures).

To estimate the Nikuradse equivalent sand roughness k_s of the gravel bed in the study reach, 60 cobbles were randomly collected on three sampling occasions. Grain size distributions were computed from the diameters in the vertically oriented axis of the 180 sampled cobbles

after Wiberg & Smith (1991). Then, the single roughness height $\Delta = d_{84}$ (d_{84} is the grain size value where 84% of the bed is finer) was considered to estimate the Nikuradse equivalent sand roughness $k_s = 3 - 3.5 \Delta$ (Griffiths, 1981; Bathurst, 1982; Bray, 1982; Wiberg & Smith, 1991; Pitlick, 1992).

A number of methods are available in literature to infer friction velocity u_* from field observations (*e.g.* Wiberg & Smith, 1991; Nezu & Nakagawa, 1993; Wilcock, 1996; Nikora *et al.*, 2001). In this study, when h was much greater than Δ ($h/\Delta \geq 15$), u_* was inferred from the log-wake law formulae (Eqns 1–2):

$$\frac{U}{u_*} = \frac{1}{\kappa} \ln\left(\frac{z-d}{k_S}\right) + A + w\left(\frac{z}{h}\right) \quad (1)$$

$$w\left(\frac{z}{h}\right) = \frac{2\Pi}{\kappa} \sin^2\left(\frac{\pi z}{2h}\right) \quad (2)$$

where z is the distance from the bed, U is the flow velocity at z, κ is the Von Karman constant (κ = 0.4), d is the displacement length [also known as a zero-plane displacement $d = 0.75k_s$ (Jackson, 1981; Nezu & Nakagawa, 1993)], A is a constant that depends on flow regime [A = 8.5 for fully rough flow, *i.e.* with a roughness Reynolds number $k^+ > 70$ (see *e.g.* Nezu & Nakagawa, 1993)] and $w(z/h)$ is a wake function estimating the deviation from the standard log-law of the velocity profile in the outer region ($z/h > 0.2$), after Coles (1956). Π is Coles' wake strength parameter which depends on Re$_*$ = $u_* h/v$, a Reynolds number depending on friction velocity (Nezu & Nakagawa, 1993).

During low-flow periods, when the ratio h/Δ was <15, Eqn 3 from Wiberg & Smith (1991) was followed, which found a log-linear relationship between the mean velocity normalised by shear velocity $\overline{U}/u_*$ and the ratio h/Δ, despite the fact that velocity profiles deviate from logarithmic law:

$$\frac{\overline{U}}{u_*} = 2.4 \ln\left(\frac{h}{\Delta}\right) + 2.04 \quad (3)$$

Numerical model description

The structure of the differential equation developed by Uehlinger *et al.* (1996) was combined with the additional term developed by Boulêtreau *et al.* (2006) to describe autogenic detachment. Furthermore, a simple function was added to the resulting equation to describe the loss by invertebrate feeding activity as estimated in this study. Note that the flow discharge Q was replaced by friction velocity u_* as the external variable forcing the detachment (Graba *et al.*, 2010).

In the resulting differential Eqn 4, B (g AFDM m^{-2}) is the epilithic biofilm biomass, t (days) is the time, T (°C) is the mean daily temperature, T_0 is the reference temperature biomass (20 °C), I (E m^{-2}) is the daily integrated light intensity, and B_0 is the minimal biomass that allows the epilithic biofilm community to recover, after Uehlinger et al. (1996).

$$\frac{dB}{dT} = G - D - L_{Gr} \tag{4}$$

$$\frac{dB}{dt} = \underbrace{\mu_{max}B}_{G1}\underbrace{\frac{1}{1+k_{inv}B}}_{G2}\underbrace{\exp(\beta(T-T_0))}_{G3}\underbrace{\frac{I}{I+k_I}}_{G4}$$
$$- \underbrace{C_{det}u_*(B-B_0)}_{D1} - \underbrace{K_{flood}u_*(B-B_0)}_{D2}$$
$$- \underbrace{C_{auto}B_b(B-B_0)}_{D3} - \underbrace{TFN_{Gr}}_{L_{Gr}}$$

G is the growth function of the equation and is formed by several terms. $G1$ describes the exponential increase in biomass, where μ_{max} (day^{-1}) is the maximum specific growth rate at the reference temperature T_0. $G2$ describes the effect of density limitation, where k_{inv} (m^2 g^{-1}) is the inverse half-saturation coefficient. This term accounts for the limitation of biofilm growth rate with increasing epilithic mat thickness due to light and nutrient limitation in the inner layers of the biofilm. $G3$ and $G4$ are other biofilm growth limitation terms that consider the effects of temperature and light, respectively. In these, β (°C^{-1}) is the coefficient of temperature dependence and K_I (E m^{-2}) is the light half-saturation coefficient.

D is the detachment function of the equation, also composed by several terms. $D1$ describes the chronic detachment, driven here by C_{det} (s m^{-1} day^{-1}) which is an empirical detachment coefficient, u_* and B. $D2$ describes the catastrophic detachment during bed-moving spates when u_* is higher than a critical friction velocity u_{*crit}, leading to a massive biofilm detachment correlated with the empirical coefficient K_{flood} (s m^{-1} day^{-1}), which is equal to K_{cat} (s m^{-1} day^{-1}) during spates (K_{cat} was calibrated in the context of very-high-flow friction velocities). K_{flood} was established (Eqn 5) using the mean velocity profiles measured in nine mountain streams in Colorado (Marchand, Jarrett & Jones, 1984), with a log-normal distribution of the gravel bed (which is also the case in this study site).

$$K_{flood}(u_*) = \begin{cases} 0 & \text{for } u_* < u_{*crit} \\ k_{cat} & \text{for } u_* \geq u_{*crit} \end{cases} \tag{5}$$

In Eqn 4, $D3$ describes autogenic detachment, also called the self-generated detachment, which is a sizeable and sudden detachment of biofilm due to a reduced resistance of the mat to floating and drifting. This occurs when biofilm becomes thicker and less cohesive with the senescence of deeper algal layers. This autogenic detachment is mainly triggered by a temperature-driven bacterial degradation of the biofilm matrix. Hence, $D3$ depends on biofilm standing stock (thus proportional to $B - B_0$) and on an empirical autogenic detachment coefficient C_{Auto} (cells^{-1} m^2) linked to the active bacterial density Bb (cells m^{-2}) (see Boulêtreau et al., 2006). B_b is described by a differential equation (Eqn 6) composed by a growth term and a loss term:

$$\frac{dB_b}{dt} = \left[\underbrace{\mu_{B_b}\exp(\beta_{B_b}(T-T_0))}_{G_{B_b}} - \underbrace{C'_{det}B}_{D_{B_b}} \right] B_b \tag{6}$$

The growth term G_{B_b} is expressed as an Arrhenius or Van't Hoff equation where μ_{B_b} (day^{-1}) is the maximum specific growth and β_{B_b} (°C^{-1}) is the coefficient of temperature. The loss term D_{B_b} is a detachment term related to the biofilm biomass loss. Other types of loss (death, lysis) were included in μ_{B_b} (Boulêtreau et al., 2006).

The last term L_{Gr} in Eqn 4 represents the loss due to our estimation of biofilm-dwelling invertebrate feeding activity, considered equal to TFN_{Gr} (g AFDM m^{-2} day^{-1}).

Validation of the model

The differential Eqns 4–6 were solved numerically by coding a fourth-order Runge-Kutta method in Fortran 90. Preliminary tests demonstrated that a time step fixed at 3 h was a good condition to reduce errors caused by numerical integration. Values of the input friction velocity u_* at each time step were obtained by linear interpolation of the measured data. Since Eqn 4 – inferred from the model of Uehlinger et al. (1996) – does not consider colonisation, the colonisation process was described by an initial condition for the biomass. Hence, a numerical parameterisation was considered following Belkhadir, Capdeville & Roques (1988) to determine the value of the initial epilithic biomass (denoted B_{init}). B_0 was set to 0, a parameter found unnecessary after checking and subsequently omitted from the calibration. The initial value $B_{b_{init}}$ was fixed in accordance with previous studies showing that epilithic bacterial densities in this study site accounted on average for 3×10^{10} cells g AFDM^{-1} (Lyautey et al., 2003, 2005a; Boulêtreau et al., 2006).

Two indices were used to test the performance of the model and the agreement between measured and simulated results. These were the χ^2 of conformity (Eqn 7; Uehlinger *et al.*, 1996) and the Nash–Sutcliffe efficiency coefficient E (Eqn 8; Lekfir, Benkaci Ali & Dechemi, 2006; Kliment, Kadlec & Langhammer, 2007):

$$\chi^2 = \sum_{i=1}^{N} \left(\frac{B(t_i) - B_{\text{meas},i}}{\text{ES}_{\text{meas},i}} \right)^2 \tag{7}$$

$$E = 1 - \frac{\sum_{i=1}^{N} \left(B_{\text{meas,i}} - B(t_i) \right)^2}{\sum_{i=1}^{N} \left(B_{\text{meas,i}} - \overline{B_{meas}} \right)^2} \tag{8}$$

where $B_{\text{meas},i}$ is the measured biomass and $B(t_i)$ is the predicted biomass at time i. $\text{ES}_{\text{meas},i}$ is the standard error in $B_{\text{meas},i}$, $\overline{B_{meas}}$ is the average of all measured values and N is the number of measurements. Generally the model is deemed perfect when E is >0.75, satisfactory when E is between 0.36 and 0.75 and unsatisfactory when E is <0.36 (Krause, Boyle & Base, 2005).

Results

Environmental background and annual dynamics of biofilm biomass

Active radiation (I) showed a typical seasonal cycle ranging from 3 to 70 E m^{-2} per day (Fig. 1a), while mean daily water temperature ranged from 4 to 25 °C (Fig. 1b). The river had two stable low-flow periods during the study (September–late October 2008 and July–September 2009) interrupted by an hydrologically disturbed period (with discharge peaking at 814 m^3 s^{-1}; Fig. 2). Epilithic biofilm biomass showed six successive peaks (stars on Fig. 2), corresponding to six separable cycles of overall biofilm growth with successive AFDM maxima of 31.5, 28.5, 58.3, 55.4, 39.7 and 34.7 g m^{-2}.

Biofilm diatom community

In terms of biomass, diatoms largely dominated the biofilm phototrophic community over the entire study period (see Majdi *et al.*, 2011). Depending on the sampling
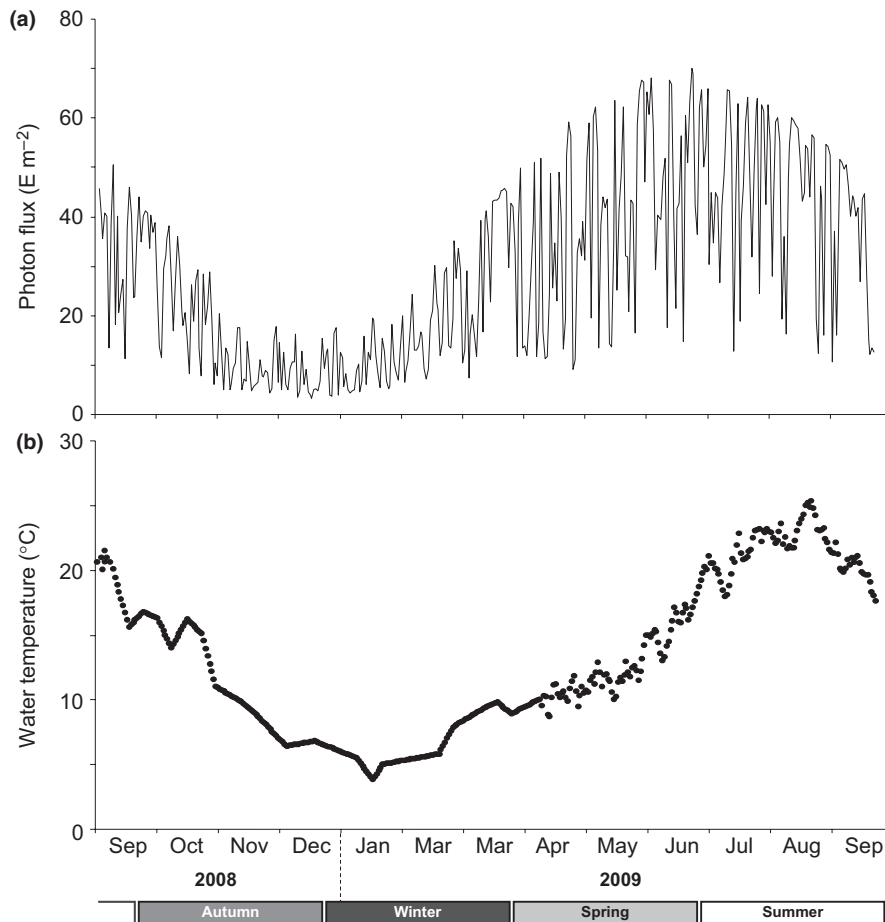
Fig. 1 Daily integrated photosynthetically active photon flux (a) and mean daily water temperature (b) during the study period.
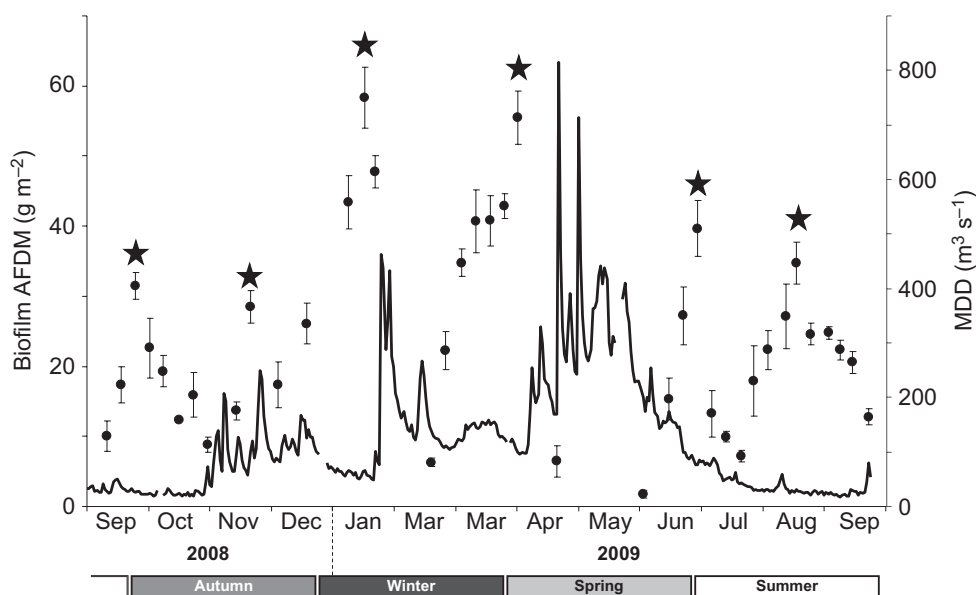
Fig. 2 Points are the mean (±1 SE, $n = 4$) ash-free dry mass (AFDM) of the epilithic biofilm; stars show peaks of biofilm growth cycles; the bold line is the mean daily discharge (MDD) during the study period.

Table 1 Relative abundance (%) and functional type of the diatom taxa contributing >5% in at least one sampling occasion

Main diatom species	Morphotype	Oct. 2008 7th	Oct. 2008 15th	Nov. 2008 12th	Nov. 2008 19th	Jan. 2009 7th	Feb. 2009 24th	Mar. 2009 25th	Apr. 2009 20th	June 2009 15th	July 2009 13th	Aug. 2009 12th	Sep. 2009 8th	Sep. 2009 22nd	Mean (%)
Achnanthidium biasolettianum	FU	4.6	3.6	12	2.6	4.2	19.3	8.9	4.2	48.1	11.4	4.2	1.4	1.0	9.7
Achnanthidium minutissimum	FU	7.0	11.3	10.3	4.2	3.5	12.3	12.5	13.7	3.2	7.3	6.2	15.2	56.8	12.6
Cocconeis pediculus	FU	3.1	4.3	2.2	0	0	0	0.2	0.5	0.2	4.4	7.7	2.1	1.9	2.1
Cocconeis placentula	FU	9.2	10.7	8.1	0.9	0.9	0.2	0.2	0	0	0	3.5	0	0	2.6
Cocconeis placentula var. euglypta	FU	0	0	0	0	0	0	0	0.2	0	11.1	5.0	6.4	2.9	2.0
Cocconeis placentula var. lineata	FU	0	0	0	0	0	0	0	0.2	0.9	18.6	5.0	2.4	0	2.1
	Tot FU	23.9	29.9	32.5	7.7	8.6	31.8	21.9	18.8	52.4	52.7	31.5	27.5	62.5	30.9
Cyclotella atomus	C	1.9	0.2	0	0.2	0	0	0	0	0	0	17.4	32.0	15.0	5.1
Cymbella cistula	C	1.5	0.9	0	0.2	0.2	10.7	4.0	1.9	0.2	0	1.5	0.7	0.5	1.7
Cymbella helvetica	C	0	0	0	0	6.1	0	0	1.4	0	0	0	0	0	0.6
Diatoma moniliformis	C	0	0	0	0	0.9	1.1	12.3	6.4	0	0	0	0	0	1.6
Diatoma vulgaris	C	9.4	7.5	5.4	3.2	1.9	0.9	4.2	5.4	0.9	1.7	4.7	1.7	1.4	3.7
Encyonema minutum	C	1.7	5.4	5.4	6.7	10.0	1.1	11.6	13.4	9.3	4.1	0.3	1.0	1.2	5.5
Gomphonema olivaceum	C	0	0.2	0	0.2	0.2	5.2	14.7	6.4	11.4	9.2	0	0	0	3.7
	Tot C	14.5	14.3	10.8	10.6	19.3	19.1	46.9	34.8	21.9	15.0	23.8	35.3	18.1	21.9
Melosira varians	Tot F	25.9	7.5	13.0	7.4	1.2	0.2	1.6	4.0	2.5	5.1	17.4	4.5	0.2	7.0
Navicula cryptotenella	FrU	4.6	8.6	2.4	4.6	9.3	10.9	3.6	7.3	1.6	5.3	1.2	2.6	3.6	5.1
Navicula tripunctata	FrU	4.6	8.4	10.0	6.9	3.0	2.1	1.8	6.4	0	1.2	0	0.7	0	3.5
Nitzschia dissipata	FrU	5.3	6.3	2.4	17.8	25.9	16.4	2.9	2.8	0.5	1.2	2.2	7.8	1.0	7.1
Nitzschia fonticola	FrU	3.4	3.4	5.6	21.1	15.2	11.8	7.4	6.6	3.2	1.5	1.2	2.6	0	6.4
	Tot FrU	17.9	26.8	20.5	50.5	53.4	41.1	15.6	23.1	5.2	9.18	4.7	13.7	4.53	22.0

Functional type abbreviations: C, colonial; F, filamentous; FU, fixed unicellular; and FrU, free unicellular (Krammer & Lange–Bertalot, 1991; Leflaive *et al.*, 2008).
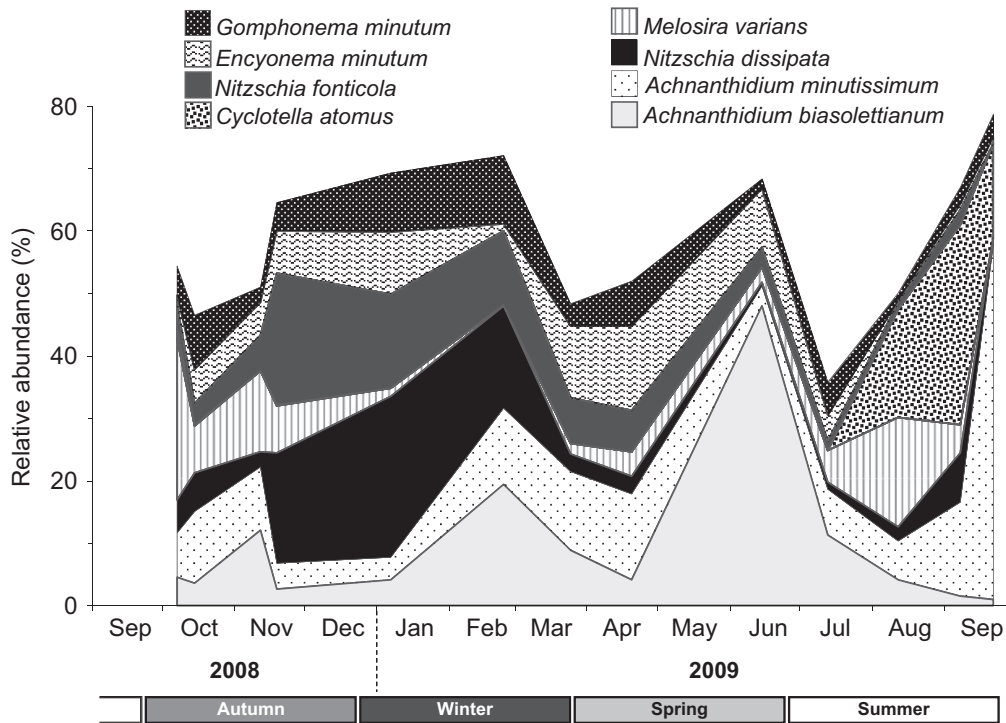
Fig. 3 Contributions (%) of the eight dominant diatom taxa to diatom assemblage during the study period.

occasion, the richness of diatom species ranged from 25 to 44 taxa in the biofilm. Of these, 18 taxa showed a relative abundance >5% in at least one sampling occasion (Table 1), and eight of these 18 taxa showed a mean relative abundance >5% (their dynamics are displayed in Fig. 3). *Achnanthidium minutissimum* was a dominant species and on average contributed to 12.6% (up to 56.8%) of the diatom assemblage. *Achnanthidium biasolettianum* contributed 9.7%, but peaked at 48.6% after snowmelt floods. *Melosira varians* contributed 7% and was more abundant during the low-flow periods. *Cyclotella atomus* (average contribution of 5.1%) also reached maxima (up to 32%) during the low-flow periods. In contrast, *Nitzschia dissipata* and *Nitzschia fonticola* (contribution of 7.1 and 6.4%, respectively) showed rela-

tively abundant maxima during the early high-flow period. Contributions of *Encyonema minutum* and *Navicula cryptotenella* to diatom assemblages averaged 5.5 and 5.1%, respectively.

Biofilm-dwelling invertebrate grazing pressure

Most nematodes inhabiting the biofilm belonged to the species *Chromadorina bioculata* and *Chromadorina viridis* (Majdi *et al.*, 2011). These two species consume biofilm diatoms and possibly their polymeric exudates (Majdi, Tackx & Buffan-Dubau, 2012c; Majdi *et al.*, 2012b). Although extremely abundant within the biofilm (on average 181 859 and up to 613 437 individuals m^{-2}), their low individual biomass made their estimated mean
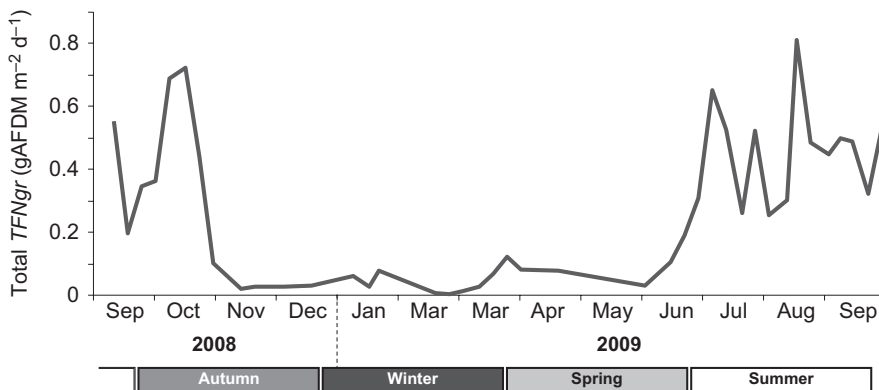

Fig. 4 Mean (n = 4) total food needs (TFN$_{gr}$) of the main biofilm-dwelling invertebrates (Nematodes, Chironomidae and Trichoptera larvae) during the study period.

feeding activity at $TFN_{gr} = 27$ (0.03–126) mg AFDM m^{-2} day^{-1}, which is relatively low compared to that of Chironomidae: $TFN_{gr} = 152$ (2–553) mg AFDM m^{-2} day^{-1} and Trichoptera larvae: $TFN_{gr} = 131$ (4.5–394) mg AFDM m^{-2} day^{-1}. The total estimated feeding activity of biofilm-dwelling invertebrates (Fig. 4) was particularly high during the summer/autumn low-flow period (up to 724 and 810 mg AFDM m^{-2} day^{-1} in mid-October 2008 and mid-August 2009, respectively).

Hydrodynamic and boundary layer parameters

The grain size distribution, established using the vertically oriented axis of cobbles, followed a log-normal distribution and gave a value of the 84th percentile size $d_{84} = 5.45$ cm. During the low-flow period ($h_{min} = 0.2$ m), an estimation of u_* with the approximation of rectangular uniform flow from $u_* = \sqrt{ghS}$ gave a value of $Re_{*min} = 8800 > 2000$ (the slope $S = 0.1\%$). According to this, at the highest regime, there was a value of $Re_* > Re_{*min} > 2000$. Therefore, Eqns 1 and 2 were used to estimate the friction velocity, with values of the longitudinal velocity U linked to $z = 0.4$ h ($U_{40\%}$) and $\Pi = 0.2$ ($Re_* > 2000$) (see Nezu & Nakagawa, 1993). The data record of daily $U_{40\%}$ was estimated by interpolation and extrapolation in a polynomial correlation ($U_{40\%} = 0.0001$ $Q^2 - 0.0024$ $Q + 0.1416$, $R^2 = 0.93$) between the weekly measured values of $U_{40\%}$ and the corre-
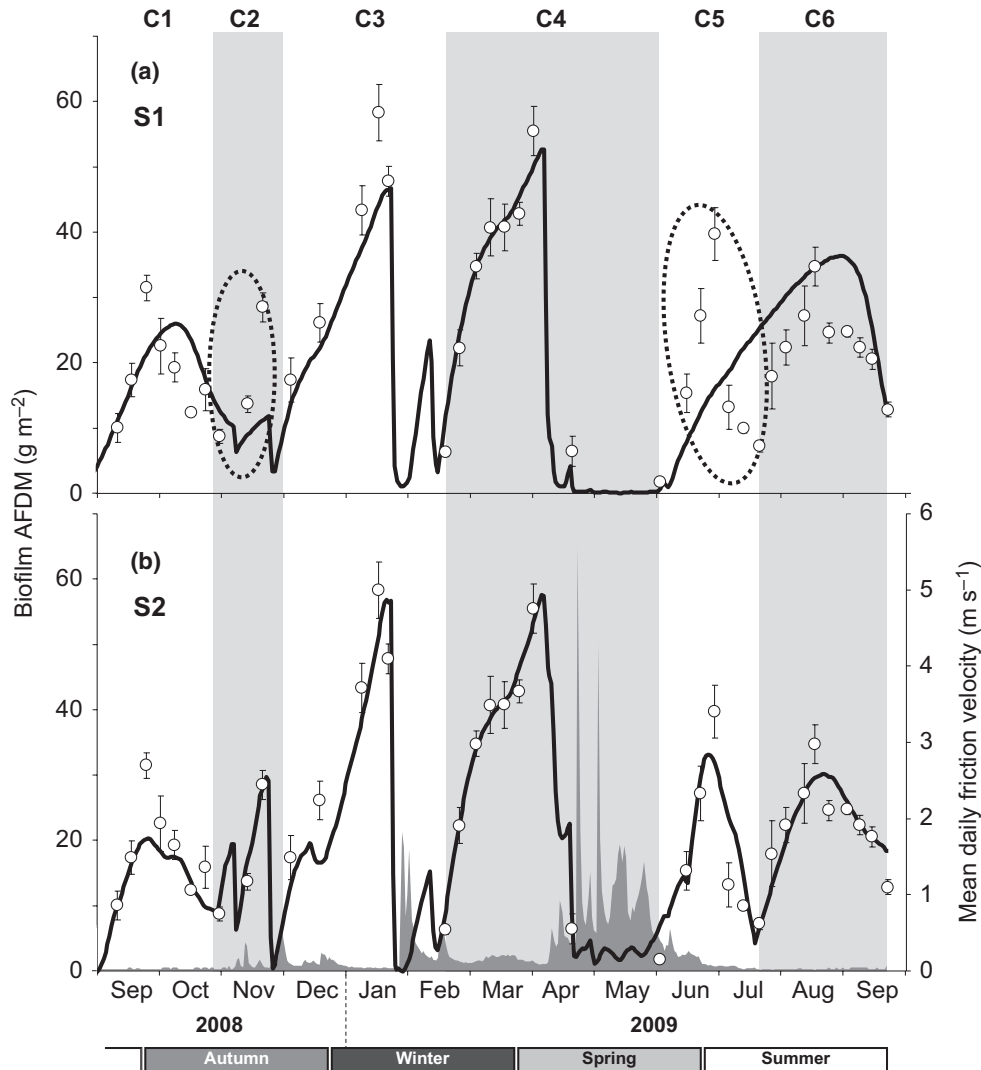
Fig. 5 (a) Results of the first simulation (S1): comparison between mean observed biofilm ash-free dry mass (AFDM) dynamics (±SE, $n = 4$) and S1 simulated AFDM (bold line; $\chi^2 = 3.172$ and $E = 0.61$). The alternation between clear and slightly shaded areas (C1–C6) represents the subdivision of the study period according to the six cycles comprising a growth phase followed by a detachment phase. The growth cycles C2 and C5 (circled by dotted line) were not reproduced by S1. (b) Results of the second simulation (S2): comparison between mean observed biofilm AFDM dynamics (±SE, $n = 4$) and S2 simulated AFDM (bold line; $\chi^2 = 486.4$ and $E = 0.84$). The dark area represents the mean daily friction velocity dynamics (u_*).

Table 2 Values of the empirical parameters found in simulations S1 and S2 (C1 to C6: growth cycles 1–6)

Simulation	μ_{max}	k_{inv}	β	k_I	C_{det}	u_{*crit}	K_{flood}	C_{auto}	μ_{B_b}	β_{B_b}	C'_{det}
S1	1	0.90	−0.08	1	0.5	0.37	1.6	4.5×10^{-14}	0.1	0.1	0.4
S2 C1	1	0.52	−0.08	1	0.80	0	0	9.5×10^{-14}	0.1	0.1	25×10^{-4}
S2 C2	1	0.70	−0.08	1	0.60	0.45	5.0	1×10^{-14}	0.1	0.1	25×10^{-4}
S2 C3	1	1.00	−0.08	1	0.70	0.33	1.0	1×10^{-14}	0.1	0.1	25×10^{-4}
S2 C4	1	1.00	−0.08	1	0.20	0.35	0.2	2×10^{-14}	0.1	0.1	25×10^{-4}
S2 C5	1	0.15	−0.08	1	0.15	0	0	3×10^{-14}	0.1	0.1	25×10^{-4}
S2 C6	1	0.50	−0.08	1	0.80	0	0	5×10^{-14}	0.1	0.1	25×10^{-4}

sponding values of mean daily discharge. During low flow, the values of mean daily velocities $\overline{U}$ used in Eqn 3 were interpolated or extrapolated from a polynomial correlation between measured velocities and corresponding mean daily discharge ($\overline{U} = 10^{-3}Q^2 + 31 \times 10^{-3}Q^2 + 1549 \times 10^{-4}$, $R^2 = 0.91$). Finally, the daily friction velocities thus obtained are displayed as the dark background area to Fig. 5b.

Model testing and evaluation

In a first simulation of biofilm AFDM dynamics, the aim was to simulate values that agreed most closely with measured values (to minimise χ^2 and optimise E). Hence, the model (using Eqns 4–6) was calibrated with the initial biomass value $B_{init} = 1$ g AFDM m^{-2} and by adjusting the values of the 11 empirical parameters (μ_{max}, K_{inv}, β, k_I, C_{det}, K_{flood}, u_{*crit}, C_{auto}, μ_{B_b}, β_{B_b} and C_{det}') in the range of values reported from field, laboratory and modelling studies (Auer & Canale, 1982; Borchardt, 1996; Uehlinger *et al.*, 1996; Lyautey *et al.*, 2005a,b; Boulêtreau *et al.*, 2006, 2008; Labiod, Godillot & Caussade, 2007), using observations regarding biofilm structure and aspect during *in situ* measurements and previous experience and knowledge of model sensitivity to a change in parameters (Graba *et al.*, 2010, 2012). The result of this first simulation (S1) is shown as a bold line in Fig. 5a, and the values of the empirical parameters used in this simulation are presented in Table 2. The year-long study was divided into six biofilm growth/detachment cycles, named C1 to C6. Each cycle consisted of a phase of growth followed by detachment. The mean values of friction velocity u_* (m s^{-1}) were estimated during the growth phases of the six cycles of biofilm growth. There, u_* ranged from 0.021 m s^{-1} during low-flow periods to 0.207 m s^{-1} during high-flow periods (see as dark background in Fig. 5b). In S1, the model correctly simulated four of the six growth cycles, with a Nash-Sutcliffe efficiency coefficient value E equal to 0.51, which corresponds to a satisfactory simula-
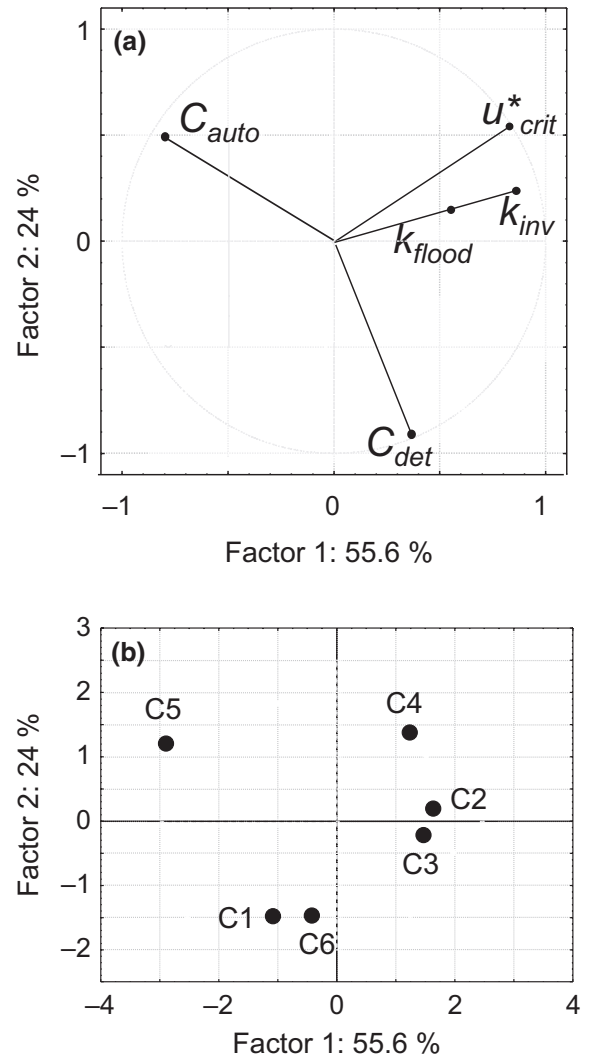
Fig. 6 Biplots from the principal component analysis (PCA), showing (a) the projection of the modelling parameters in the factorial plane of the PCA: the inverse half-saturation coefficient K_{inv} (g^{-1} m^2), the chronic detachment coefficient C_{det} (s m^{-1} day^{-1}), the critical velocity u_{*crit} (m s^{-1}), the empirical coefficient of catastrophic detachment K_{flood} (s m^{-1} day^{-1}) and the autogenic detachment coefficient C_{auto} (cells^{-1} m^2), and (b) the location of the six growth cycles (C1–C6) in the factorial plane of the PCA.

tion (Krause *et al.,* 2005). However, two cycles of growth/detachment of the biofilm (C2 and C5 circled by dotted line on Fig. 5a) were not reproduced by S1. The analysis of the temporal dynamics of diatom taxa classified according to their morphological type (Table 1) showed that the two growth cycles not reproduced by S1 were characterised by the predominance of fixed unicellular (FU) diatoms, which grow firmly attached to the substratum. This suggests that FU diatoms can overcome high hydrodynamic drag and shear stress while filamentous forms cannot (Wehr & Sheath, 2003; Tornés & Sabater, 2010).

A second simulation (S2) was performed with different values of the following empirical parameters (K_{inv}, C_{det}, K_{flood}, u_{*crit} and C'_{det}) for each of the six biofilm growth cycles. The result of this simulation is presented as a bold line in Fig. 5b, and the corresponding parameter values are detailed in Table 2. With S2, the two growth cycles which were not reproduced by S1 (circled in Fig. 5a) were reproduced more effectively (Fig. 5b), with better Nash-Sutcliffe efficiency coefficient values $E = 0.89$ (>0.75), corresponding to a perfect modelling *sensu* Krause *et al.* (2005).

A principal component analysis (PCA) was performed to analyse parameter (k_{inv}, C_{det}, K_{flood}, u_{*crit} C_{auto} and μ_{B_b}) value distribution over the six biofilm growth cycles (Fig. 6a). This PCA distinguished four groups of growth cycles (Fig. 6b): C1–C6, C2–C3, C4 and C5 in a plane of axis, explaining 55.6% of the variance in the first factor (the inverse half-saturation coefficient: k_{inv}) and 24% of the variance in the second factor (the chronic detachment coefficient: C_{det}).

Discussion

In this study, the combined effects of local hydrodynamics, biofilm-dwelling grazers and diatom functional diversity on biofilm growth patterns were modelled. Rather than using a single set of parameters throughout the study period, epilithic biofilm biomass dynamics were modelled with variable parameterisation, considering the variation of biofilm composition, structure and physical characteristics (*i.e.* parameterisation is contingent upon growth cycle characteristics). Despite the fact that degrees of freedom decreased with the S2 approach (allowing predicted values to be compared with three to nine observational measures), the model's ability to predict biofilm growth patterns is reliable in various hydrological scenarios. Some parameters remained fairly constant throughout the six growth cycles (Table 2), such as bacterial and biomass maximum-specific growth rate coefficients (μ_{B_b} and μ_{max}, respectively). It is likely that this constancy was a result of the steady nutrient availability from the anthropogenic inputs to the Garonne (Teissier *et al.*, 2002, 2007). Model sensitivity to light – as assessed by the light half-saturation coefficient k_I (E m^{-2}) – also remained constant, probably due to unlimited irradiance at the Garonne study site. For greater clarification, the remaining findings will be discussed after arranging the six biofilm annual growth cycles highlighted into four defined groups (Fig. 6b) with comparable biofilm biomass patterns.

Biofilm growth under stable low flow

The first group was composed of growth cycles C1 and C6, which corresponded to biofilm growing under low-flow periods with important biomass loss attributed to chronic detachment ($C_{det} = 0.8$ s m^{-1} day^{-1}). The filamentous diatom *Melosira varians* (25.9%) dominated during C1 and linear colonies of the tychoplanktonic *Cyclotella atomus* (32%) dominated during C6. Both these diatoms show no attachment mechanisms or structures of any sort. The inverse half-saturation parameter values k_{inv} (g^{-1} m^2), which accounted for the limitation of the biomass growth rate with increasing mat thickness, were very close between C1 and C6 ($k_{inv} = 0.52$ and 0.5, respectively). Corresponding biomass maxima observed for C1 and C2 were also similar (31.5 and 34.7 g AFDM m^{-2}, respectively). Furthermore, it was observed that the small and firmly attached *Achnanthidium minutissimum* persisted at the end of these two growth cycles.

While catastrophic detachment did not occur in this first group of growth cycles, autogenic detachment was significant. This makes sense since bacterial activity is especially intense at high temperatures recorded in the summer/autumn (Lyautey *et al.*, 2010) and can destabilise deeper biofilm layers (Boulêtreau *et al.*, 2006). Our estimation of invertebrate feeding activity was also highest for this first group of growth cycles. However, it was estimated that the daily removal of biofilm was (on average) just 1% of the available biomass, with a maximum of 6% recorded on 17 August 2009. Thus, as reported by Lyautey *et al.* (2005a) and Boulêtreau *et al.* (2006), it can be confirmed that during warm, undisturbed periods, it is predominantly autogenic factors that drive the patterns of biofilm dynamics in this system.

Biofilm growth under a variable flow regime

The second group of growth cycles consisted of C2 and C3, which occurred during moderate-to-high flow from

November 2008 to January 2009. During both cycles, free unicellular (FrU) diatom taxa prevailed. These FrU were comprised mainly of *Nitzschia dissipata* and *N. fonticola*, which are fast-growing diatoms maintaining close contact with various surfaces with their raphe system (Wehr & Sheath, 2003; Cardinale, 2011). During C2 and C3, chronic detachment was more significant, with values of C_{det} = 0.6 and 0.7 s m^{-1} day^{-1}, respectively. While autogenic detachment and grazing pressure were negligible, the spates occurring at the end of these two growth cycles induced a catastrophic loss of biofilm.

In fact, the critical friction velocities causing this catastrophic detachment were u_{*crit} = 0.45 and 0.33 m s^{-1} in C2 and C3, respectively. The empirical coefficients of detachment were K_{flood} = 5 and 1 s m^{-1} day^{-1} in C2 and C3, respectively. This means that, even when showing comparable FrU-dominated diatom assemblages, the biofilm growing during C2 (under a mean friction velocity of u_* = 0.124 m s^{-1}) was more resistant to shear stress than the biofilm growing during C3 under less extreme hydrodynamic conditions (u_* = 0.087 m s^{-1}). This result is consistent with the findings of Graba *et al.* (2013) in experimental flumes, where the resistance of biofilm to detachment depends greatly on the local hydrodynamic conditions on the boundary layer where it has grown. In other words, attached biomass is detached as soon as friction velocity exceeds the velocity exerted during the growth phase.

The different hydrodynamical resistance of C2 and C3 biofilms could also be explained by the very high densities of nematodes dwelling in the latter (Majdi *et al.*, 2012a). As shown by the estimations in this study, the feeding impact of nematodes is low. However, their presence in the mat seems to affect key biofilm processes such as oxygen turnover (Mathieu *et al.*, 2007), metabolite release (Sabater *et al.*, 2003) and detachment (Gaudes *et al.*, 2006). It is possible that their high abundance (and hence their bioturbation effects) could have substantially reduced biofilm matrix cohesion, thus favouring biofilm detachment by shear stress. This supports the general hypothesis that the direct top-down control of biofilm by nematodes (and meiofauna in general) is not a primary regulating mechanism, while the indirect drilling influence of these small invertebrates on mat architecture seems more significant (Pinckney *et al.*, 2003). On the opposite, other invertebrates that secrete silky retreats (such as Psychomyiidae larvae) or sticky mucous threads (such as flatworms) are expected to 'consolidate' the cohesion of biofilm matrix (see *e.g.* Stief & Becker, 2005; Ings, Hildrew & Grey, 2012; Majdi *et al.*, 2014). Therefore, in this context, we recommend that the bioturbation and/or

'consolidation' potential of biofilm-dwelling organisms should be carefully considered in future efforts to model biofilm growth patterns.

Biofilm growth under a stable high flow

The third group of growth cycles concerned only the biofilm growth cycle C4, which occurred under stable winter high flow. This was dominated by colonial diatoms, such as *Encyonema minutum* and *Gomphonema olivaceum*, which form colonies within mucilaginous tubes enabling adherence and growth even under relatively fast flow (u_* = 0.193 m s^{-1} during the growth phase). During C4, chronic detachment was low (C_{det} = 0.2 s m^{-1} day^{-1}) and autogenic detachment and grazing were negligible, but the catastrophic detachment caused an important loss of biofilm biomass when friction velocity exceeded the critical value of 0.35 m s^{-1}.

In the Garonne, Majdi *et al.* (2012a) observed a massive detachment of epilithic biofilm under streambed flow velocities >0.3 m s^{-1}. Biggs, Goring & Nikora (1998) also observed important biofilm losses when flow velocity exceeded 0.2 m s^{-1} in New Zealand streams. Furthermore, data obtained in experimental flow troughs (Poff *et al.*, 1990) reported considerably lower biofilm biomass under high (0.3–0.4 m s^{-1}) versus slow (<0.2 m s^{-1}) flow regimes. Therefore, the results in this study, together with evidence from the literature, support the finding that stream epilithic biofilm development in the Garonne during this study period is mainly driven by hydrological forces when streambed flow velocity approaches and exceeds 0.3 m s^{-1}.

Biofilm recovery after critical snowmelt floods

Finally, the last group was the growth cycle C5, a fast-growth cycle occurring just after the spring snowmelt floods (u_* = 0.207 m s^{-1} during the growth phase). During C5, biofilm losses by chronic detachment and the inverse half-saturation parameter were low (C_{det} = 0.15 s m^{-1} day^{-1} and k_{inv} = 0.15 g^{-1} m^2). Fixed unicellular diatoms, *Achnanthidium biasolettianum* and *Cocconeis placentula*, dominated during C5. These diatoms can firmly adhere to the substratum under high-flow constraints and are characteristic of early successional stages (Wehr & Sheath, 2003). There was no flow-induced catastrophic biomass loss during C5. However, large-sized biofilm-dwelling invertebrates: mostly highly mobile Heptageniidae ephemeropterans and gallery-building psychomyiid trichopterans crowded the cobbles from mid-June onwards (Majdi *et al.*, 2012a).

Although the estimated feeding activity of biofilm-dwelling invertebrates was relatively significant during C5 (up to 0.65 gAFDM m^{-2} day^{-1} in early July), feeding *per se* did not explain the major loss of biofilm observed at the end of this growth cycle (from 40 g AFDM m^{-2} on 29 June to 7 g AFDM m^{-2} on 21 July 2009). However, once again, it seems likely that the presence of active invertebrates foraging in and disturbing the biofilm could have favoured its detachment. Another plausible rationale for this loss is strong grazing pressure exerted by more mobile grazers: *for example,* Heptageniidae mayflies, fish (see Van Dam *et al.*, 2002), which were not sampled in our study. Alternatively, in this simulation, the loss of biofilm biomass was mainly attributed to bacterial-induced autogenic detachment, especially under temperature maxima (Boulêtreau *et al.*, 2006). Hence, during C5, autogenic detachment was high ($C_{auto} = 3 \times 10^{-12}$ cells^{-1} m^{-2}), probably because of a combination of high bacterial and invertebrate activity within the mat.

By regarding biofilm dynamics as a combination of growth and detachment phases in a fluctuating environment, the modelling approach in this study adequately reproduced a biofilm biomass pattern over the course of a year. Thus, it was found that (i) under high-flow conditions, biofilm dynamics were governed by the allogeneic (hydrological) control of diatom ecological successions, and (ii) during low-flow periods, biofilm dynamics were governed by autogenic controls such as self-detachment and invertebrate activity. Further biofilm biomass models should consider biological forcing, such as grazing pressure by larger and more mobile organisms (*e.g.* fish and large invertebrates) and the effects of bioturbation/consolidation on biofilm autogenic detachment.

Acknowledgments

References

Abramoff M.D., Magelhaes P.J. & Ram S.J. (2004) Image processing with ImageJ. *Biophotonics International*, **11**, 36–42.

Améziane T., Garabetian F., Dalger D., Sauvage S., Dauta A. & Capblancq J. (2002) Epilithic biomass in a large gravel bed river (the Garonne, France): a manifestation of eutrophication? *River Research and Applications*, **18**, 343–354.

Andrássy I. (1956) Die Rauminhalts– und Gewichtsbestimmung der Fadenwurmer (Nematoden). *Acta Zoologica Hungarica*, **2**, 1–15.

Asaeda T. & Hong Son D. (2000) Spatial structure and populations of a periphyton community: a model and verification. *Ecological Modeling*, **133**, 195–207.

Asaeda T. & Hong Son D. (2001) A model of the development of a periphyton community resource and flow dynamics. *Ecological Modeling*, **137**, 61–75.

Auer M.T. & Canale R.P. (1982) Ecological studies and mathematical modelling of Cladophora in Lake Huron: 3. The dependence of growth rates on internal phosphorus pool size. *Journal of Great Lakes Research*, **8**, 93–99.

Bathurst J.C. (1982) Theoretical aspects of flow resistance. In: *Gravel–Bed Rivers* (Eds R.D. Hey, J.C. Bathurst & C.R. Thorne), pp. 83–108. John Wiley, New York.

Battin T.J., Kaplan L.A., Newbold J.D. & Hansen M.E. (2003) Contributions of microbial biofilms to ecosystem processes in stream mesocosms. *Nature*, **426**, 439–441.

Belkhadir R., Capdeville B. & Roques H. (1988) Fundamental descriptive study and modelization of biological film growth: I. Fundamental descriptive study of biological film growth. *Water Research*, **22**, 59–69.

Benke A.C. & Wallace J.B. (1980) Trophic basis of production among net–spinning caddisflies in a southern Appalachian stream. *Ecology*, **61**, 108–118.

Besemer K., Singer G., Hodl I. & Battin T.J. (2009) Bacterial community composition of stream biofilms in spatially variable-flow environments. *Applied and Environemental Microbiology*, **75**, 7189–7195.

Biggs B.J.F., Goring D.G. & Nikora V.I. (1998) Subsidy and stress responses of stream periphyton to gradients in water velocity as a function of community growth form. *Journal of Phycology*, **34**, 598–607.

Biggs B.J.F., Nikora V.I. & Snelder T.H. (2005) Linking scales of flow variability to lotic ecosystem structure and function. *River Research and Applications*, **21**, 283–298.

Borchardt M.A. (1996) Nutrients. In: *Algal Ecology, Freshwater Benthic Ecosystems* (Eds R.J. Stevenson, M.L. Bothwell & R.L. Lowe), pp. 183–227. Academic Press, San Diego, CA.

Boulêtreau S., Garabetian F., Sauvage S. & Sánchez–Pérez J.M. (2006) Assessing the importance of a self-generated detachment process in river biofilm models. *Freshwater Biology*, **51**, 901–912.

Boulêtreau S., Izagirre O., Garabetian F., Sauvage S., Elosegi A. & Sánchez-Pérez J.M. (2008) Identification of a minimal adequate model to describe the biomass dynamics of river epilithon. *River Research and Applications*, **24**, 36–53.

Bray D. I. (1982) Flow resistance in gravel–bed rivers. In: *Gravel–Bed Rivers* (Eds R.D. Hey, J.C. Bathurst & C.R. Thorne), pp. 109–132. John Wiley, New York.

Butkas K., Vadeboncoeur Y. & Vander Zanden M. (2011) Estimating benthic invertebrate production in lakes: a comparison of methods and scaling from individual taxa to the whole–lake level. *Aquatic Sciences*, **73**, 153–169.

Cardinale B.J. (2011) Biodiversity improves water quality through niche partitioning. *Nature*, **472**, 86–89.

Chang I., Gilbert E.S., Eliashberg N. & Keasling J.D. (2003) A three-dimensional, stochastic simulation of biofilm growth and transport-related factors that affect structure. *Microbiology*, **149**, 2859–2871.

Coles D. (1956) The low of the wake in the turbulent boundary layer. *Journal of Fluid Mechanics*, **1**, 191–226.

Costerton J.W., Lewandowski Z., Caldwell D.E., Korber D.R. & Lappin-Scott H.M. (1995) Microbial biofilms. *Annual Reviews in Microbiology*, **49**, 711–745.

Flipo N., Even S., Poulin M., Tusseau–Vuillemin M.H., Améziane T. & Dauta A. (2004) Biogeochemical modelling at the river scale: plankton and periphyton dynamics, Grand Morin case study, France. *Ecological Modeling*, **176**, 333–347.

Ford T.E. & Lock M.A. (1987) Epilithic metabolism of dissolved organic carbon in boreal forest rivers. *FEMS Microbiology Letters*, **45**, 89–97.

Fuller R.L., Roelofs J.L. & Frys T.J. (1986) The importance of algae to stream invertebrates. *Journal of the North American Benthological Society*, **5**, 290–296.

Gaudes A., Sabater S., Vilalta E. & Muñoz I. (2006) The nematode community in cyanobacterial biofilms in the river Llobregat, Spain. *Nematology*, **8**, 909–919.

Graba M., Kettab A., Sauvage S. & Sanchez-Pérez J.M. (2012) On modeling chronic detachment of periphyton in artificial rough, open channel flow. *Desalination and Water Treatment*, **41**, 79–87.

Graba M., Moulin F.Y., Boulêtreau S., Garabétian F., Kettab A., Eiff O. *et al.* (2010) Effect of near-bed turbulence on chronic detachment of epilithic biofilm in artificial rough, open channel flow: experimental and modeling approaches. *Water Resources Research*, **46**, W11531. DOI: 10.1029/2009WR008679

Graba M., Sanchez–Pérez J.M., Moulin F.Y., Urrea G., Sabater S. & Sauvage S. (2013) Interaction between local hydrodynamics and algal community in epilithic biofilm. *Water Research*, **47**, 2153–2163.

Griffiths G.A. (1981) Flow resistance in coarse gravel-bed rivers. *Journal of the Hydraulic Division*, **107**, 899–918.

Hall R.O., Likens G.E. & Malcom H.M. (2001) Trophic basis of invertebrate production in 2 streams at the Hubbard Brook Experimental Forest. *Journal of the North American Benthological Society*, **20**, 432–447.

Hillebrand H. (2009) Meta–analysis of grazer control of periphyton biomass across aquatic ecosystems. *Journal of Phycology*, **45**, 798–806.

Horner R.R. & Welch E.B. (1981) Stream periphyton development in relation to current velocity and nutrients. *Canadian Journal of Fisheries and Aquatic Sciences*, **38**, 449–457.

Horner R.R., Welch E.B. & Veenstra R.B. (1983) Development of nuisance periphytic algae in laboratory streams in relation to enrichment and velocity. In: *Periphyton of Freshwater Ecosystems* (Ed. R.G. Wetzel), pp. 121–164. Dr. W. Junk Publishers, The Hague.

Ings N.L., Hildrew A.G. & Grey J. (2012) 'House and garden': larval galleries enhance resource availability for a sedentary caddisfly. *Freshwater Biology*, **57**, 2526–2538.

Jackson C.R., Churchill P.F. & Roden E. (2001) Successional changes in bacterial assemblage structure during epilithic biofilm development. *Ecology*, **82**, 555–566.

Jackson P.S. (1981) On the displacement height in the logarithmic velocity profile. *Journal of Fluid Mechanics*, **111**, 15–25.

Kliment Z., Kadlec J. & Langhammer J. (2007) Evaluation of suspended load changes using AnnAGNPS and SWAT semi-empirical erosion models. *Catena*, **73**, 286–299.

Krammer K. & Lange–Bertalot H. (1991) *Bacillariophyceae*, Vol **1–4**, Spektrum Akademischer Verlag, Heidelberg.

Krause P., Boyle D.P. & Base F. (2005) Comparison of different efficiency criteria for hydrological model assessment. *Advances in Geosciences*, **5**, 89–97.

Labiod C., Godillot R. & Caussade B. (2007) The relationship between stream periphyton dynamics and near-bed turbulence in rough open-channel flow. *Ecological Modeling*, **209**, 78–96.

Leflaive J., Boulêtreau S., Buffan-Dubau E. & Ten–Hage L. (2008) Temporal patterns in epilithic biofilm–relation with a putative allelopathic activity. *Fundamental and Applied Limnology*, **173**, 121–134.

Lehner B., Döll P., Alcamo J., Henrichs T. & Kaspar F. (2006) Estimating the impact of global change on flood and drought risks in Europe: a continental, integrated analysis. *Climatic Change*, **75**, 273–299.

Lekfir A., Benkaci Ali T. and Dechemi N. (2006) Quantification du transport solide par la technique floue, application au barrage de Beni Amrane (Algérie). *Revue des Sciences de L'Eau*, **19**, 247–257.

Lock M.A., Wallace R.R., Costerton J.W., Ventullo R.M. & Charlton S.E. (1984) River epilithon: towards a structural-functional model. *Oikos*, **42**, 10–22.

Lyautey E., Boulêtreau S., Madigou E.Y. & Garabetian F. (2010) Viability of differentiated epilithic bacterial communities in the River Garonne (SW France). *Hydrobiologia*, **637**, 207–218.

Lyautey E., Jackson C.R., Cayrou J., Rols J.L. & Garabétian F. (2005a) Bacterial community succession in natural river biofilm assemblages. *Microbial Ecology*, **50**, 589–601.

Lyautey E., Lacoste B., Ten–Hage L., Rols J.L. & Garabétian F. (2005b) Analysis of bacterial diversity in river biofilms using 16S rDNA PCR–DGGE: methodological settings and fingerprints interpretation. *Water Research*, **39**, 380–388.

Lyautey E., Teissier S., Charcosset J.Y., Rols J.L. & Garabétian F. (2003) Bacterial diversity of epilithic biofilm assemblages of an anthropised river section, assessed by DGGE analysis of a 16S rDNA fragment. *Aquatic Microbial Ecology*, 33, 217–224.

Majdi N., Boiché A., Traunspurger W. & Lecerf A. (2014) Predator effects on a detritus-based food web are primarily mediated by nontrophic interactions. *Journal of Animal Ecology*, doi: 10.1111/1365-2656.12189

Majdi N., Mialet B., Boyer S., Tackx M., Leflaive J., Boulêtreau S. *et al.* (2012a) The relationship between epilithic biofilm stability and its associated meiofauna under two patterns of flood disturbance. *Freshwater Science*, 31, 38–50.

Majdi N., Tackx M. & Buffan–Dubau E. (2012c) Trophic positioning and microphytobenthic carbon uptake of biofilm–dwelling meiofauna in a temperate river. *Freshwater Biology*, 57, 1180–1190.

Majdi N., Tackx M., Traunspurger W. & Buffan–Dubau E. (2012b) Feeding of biofilm-dwelling nematodes examined using HPLC-analysis of gut pigment contents. *Hydrobiologia*, 680, 219–232.

Majdi N., Traunspurger W., Boyer S., Mialet B., Tackx M., Fernandez R. *et al.* (2011) Response of biofilm-dwelling nematodes to habitat changes in the Garonne River, France: influence of hydrodynamics and microalgal availability. *Hydrobiologia*, 673, 229–244.

Marchand J.P., Jarrett R.D. & Jones L.L. (1984) Velocity profile, water–surface slope, and bed–material size for selected streams in Colorado. United States Geological Survey Open–File Report 84–733, Lakewood, CO.

Mathieu M., Leflaive J., Ten–Hage L., De Wit R. & Buffan–Dubau E. (2007) Free-living nematodes affect oxygen turnover of artificial diatom biofilms. *Aquatic Microbial Ecology*, 49, 281–291.

McIntire C.D. (1973) Periphyton dynamics in laboratory streams: a simulation model and its implications. *Ecological Monographs*, 34, 399–420.

McIntire C.D. (1983) A conceptual framework for process studies in lotic ecosystems. In: *Dynamics of Lotic Ecosystems* (Eds T.D. Fontaine & S.M. Bartell), pp. 43–68. Ann Arbor Science Publishers, Ann Arbor, MI.

McIntire C.D. & Colby J.A. (1978) A hierarchical model of lotic ecosystems. *Ecological Monographs*, 48, 167–190.

McIntire C.D., Gregory S.V., Steinman A.D. & Lamberti G.A. (1996) Modeling benthic algal communities: an example from stream ecology. In: *Algal Ecology, Freshwater Benthic Ecosystems* (Eds R.J. Stevenson, M.L. Bothwell & R.L. Lowe), pp. 670–702. Academic Press, San Diego, CA.

Momo F. (1995) A new model for periphyton growth in running waters. *Hydrobiologia*, 299, 215–218.

Moulin F.Y., Peltier Y., Bercovitz Y., Eiff O., Beer A., Pen C. *et al.* (2008) Experimental study of the interaction between a turbulent flow and a river biofilm growing on macrorugosities. In: 8th ICHE Advances in hydro–science and engineering, 1887–1896.

Mulholland P.J., Steinman A.D., Palumbo A.V. & Elwood J.W. (1991) Role of nutrient cycling and herbivory in regulating periphyton communities in laboratory streams. *Ecology*, 72, 966–982.

Nezu I. & Nakagawa H. (1993) *Turbulence in Open–Channel Flows*. Balkema, Rotterdam.

Nikora V., Goring D., McEwan I. & Griffiths G. (2001) Spatially averaged open-channel flow over rough bed. *Journal of Hydraulic Engineering*, 127, 123–133.

Peterson C.G. (1996) Response of benthic algal communities to natural physical disturbance. In: *Algal Ecology, Freshwater Benthic Ecosystems* (Eds R.J. Stevenson, M.L. Bothwell & R.L. Lowe), pp. 375–403. Academic Press, San Diego, CA.

Peterson C.G. & Stevenson R.J. (1992) Resistance and resilience of lotic algal communities: importance of disturbance timing and current. *Ecology*, 73, 1445–1461.

Pfannkuche O. & Thiel H. (1988) Sample processing. In: *Introduction to the Study of Meiofauna* (Eds R.P. Higgins & H. Thiel), pp. 134–145. Smithsonian Institution Press, Washington, DC.

Pinckney J.L., Carman K.R., Lumsden S.E. & Hymel S.N. (2003) Microalgal-meiofaunal trophic relationships in muddy intertidal estuarine sediments. *Aquatic Microbial Ecology*, 31, 99–108.

Pitlick J. (1992) Flow resistance under conditions of intense gravel transport. *Water Resources Research*, 28, 891–903.

Plante C. & Downing J.A. (1989) Production of freshwater invertebrate populations in lakes. *Canadian Journal of Fisheries and Aquatic Sciences*, 46, 1489–1498.

Poff N.L., Voelz N.J., Ward J.V. & Lee R.E. (1990) Algal colonization under four experimentally controlled current regimes in high mountain stream. *Journal of the North American Benthological Society*, 9, 303–318.

Power M.E. & Stewart A.J. (1987) Disturbance and recovery of an algal assemblage following flooding in an Oklahoma stream. *American Midland Naturalist*, 117, 333–345.

Riber H.H. & Wetzel R.G. (1987) Boundary-layer and internal diffusion effects on phosphorus fluxes in lake periphyton. *Limnology and Oceanography*, 32, 1181–1194.

Romani A.M., Amalfitano S., Artigas J., Fazi S., Sabater S., Timoner X. *et al.* (2013) Microbial biofilm structure and organic matter use in Mediterranean streams. *Hydrobiologia*, 719, 43–58.

Sabater S., Vilalta E., Gaudes A., Guasch H., Munoz I. & Romani A. (2003) Ecological implications of mass growth of benthic cyanobacteria in rivers. *Aquatic Microbial Ecology*, 32, 175–184.

Saravia L., Momo F. & Boffi Lissin L.D. (1998) Modeling periphyton dynamics in running water. *Ecological Modeling*, 114, 35–47.

Sobczak W.V. (1996) Epilithic bacterial responses to variations to algal biomass and labile organic dissolved carbon

during biofilm colonization. *Journal of the North American Benthological Society*, **15**, 143–154.

Steemann-Nielsen E. (1975) *Marine Photosynthesis with Special Emphasis on Ecological Aspects*. Elsevier Scientific Publishing, Amsterdam.

Stevenson R.J. (1983) Effects of currents and conditions simulating autogenically changing microhabitats on benthic diatom immigration. *Ecology*, **64**, 1514–1524.

Stief R.J. & Becker G. (2005) Structuring of epilithic biofilms by the caddisfly Tinodes rostocki: photosynthetic activity and photopigment distribution in and beside larval retreats. *Aquatic Microbial Ecology*, **38**, 71–79.

Teissier S., Garabétian F., Torre M., Dalger D. & Labroue L. (2002) Impact of an urban centre on the nitrogen cycle processes of epilithic biofilms during a summer low-water period. *River Research and Applications*, **18**, 21–30.

Teissier S., Torre M., Delmas F. & Garabétian F. (2007) Detailing biogeochemical N budgets in riverine epilithic biofilms. *Journal of the North American Benthological Society*, **26**, 178–190.

Tekwani N., Majdi N., Mialet B., Tornés E., Urrea-Clos G., Buffan-Dubau E. *et al.* (2013) Contribution of epilithic diatoms to benthic-pelagic coupling in a temperate river. *Aquatic Microbial Ecology*, **69**, 47–57.

Timoner X., Acuna V., Von Schiller D. & Sabater S. (2012) Functional responses of stream biofilms to flow cessation, desiccation and rewetting. *Freshwater Biology*, **57**, 1565–1578.

Tornés E. & Sabater S. (2010) Variable discharge alters habitat suitability for benthic algae and cyanobacteria in a forested Mediterranean stream. *Marine and Freshwater Research*, **61**, 441–450.

Uehlinger U., Buhrer H. & Reichert P. (1996) Periphyton dynamics in a floodprone prealpine river: evaluation of significant processes by modeling. *Freshwater Biology*, **36**, 249–263.

Van Dam A.A., Beveridge M.C.M., Azim M.E. & Verdegem M.C.J. (2002) The potential of fish production based on periphyton. *Reviews in Fish Biology and Fisheries*, **12**, 1–31.

Wehr J.D. & Sheath R.G. (2003) *Freshwater Algae of North America*. Academic Press, San Diego, CA.

Wiberg P.L. & Smith J.D. (1991) Velocity distribution and bed roughness in high–gradient streams. *Water Resources Research*, **27**, 825–838.

Wilcock P. (1996) Estimating local bed shear stress from velocity observations. *Water Resources Research*, **32**, 3361–3366.

Winterbourn M.J. (1990) Interactions among nutrients, algae and invertebrates in New Zealand mountain stream. *Freshwater Biology*, **23**, 463–474.